

Accurate electronic and optical properties of bulk antiferromagnet CrSBr via a tuned hybrid density functional with on-site corrections

Ashwin Ramasubramaniam,^{1,2,*} Daniel Hernangómez Pérez,³ Javier Junquera,⁴ María
Camarasa-Gómez⁵

¹ Department of Mechanical and Industrial Engineering, University of Massachusetts, Amherst,
MA 01003, U.S.A.

² Graduate Program in Materials Science and Engineering, University of Massachusetts,
Amherst, MA 01003, U.S.A.

³ CIC nanoGUNE BRTA, Tolosa Hiribidea 76, 20018 San Sebastián, Spain

⁴ Departamento de Ciencias de la Tierra y Física de la Materia Condensada, Facultad de
Ciencias, Universidad de Cantabria, Avenida de los Castros s/n, E-39005 Santander, Spain

⁵ Centro de Física de Materiales (CFM-MPC), CSIC-UPV/EHU, Paseo Manuel de Lardizabal 5
20018 Donostia-San Sebastián, Spain

ABSTRACT

CrSBr, a layered antiferromagnet, is emerging as a versatile platform for exploring strong coupling between optical and magnetic properties in low dimensions. While experimental research on this material has progressed at a rapid pace, reliable results on the *ab initio* front are limited to the domain of self-consistent, many-body perturbation theory, which is both computationally expensive and technically challenging. We present an alternate, less-demanding approach – rooted

in generalized Kohn-Sham density functional theory – that can deliver accurate electronic structure and optical absorption spectra of CrSBr, as well as quantitatively accurate predictions of coupling of excitons to magnetic order in CrSBr. Using a minimal two-parameter set that can be tuned to reproduce a couple of well-known experimental and/or theoretical benchmarks, such as fundamental and optical gaps, we demonstrate excellent predictive capability for the tuned functional. The approach presented here can potentially be applied broadly to other magnetic semiconductors, complementing and simplifying current approaches to modeling these materials.

Keywords: CrSBr, antiferromagnetic semiconductors, layered magnets, density functional theory, correlated materials

Corresponding Author

* ashwin@engin.umass.edu

1. INTRODUCTION

Layered materials have been attracting significant research interest over a couple of decades, driven by discoveries of new materials,^{1,2} physical phenomena,^{3,4} and technological advancements.⁵⁻⁷ More recently, there has been a surge of interest in layered magnets where the unique nature of low-dimensional quasiparticle excitations, driven by quantum confinement, are further coupled to magnetic order, leading to a host of new emergent behaviors.⁸⁻¹⁵ Among layered magnets, CrSBr – an A-type antiferromagnetic semiconductor – has attracted intense scrutiny due to several intriguing properties, including strong coupling of excitons and magnons,¹⁶⁻¹⁸ strain- and gate-tunability of excitons,^{15,19} magnetically dressed exciton-polaritons,²⁰⁻²² and defect-induced magnetic phase transitions,²³ to name a few. Additionally, CrSBr is relatively stable at ambient conditions and possesses a relatively high Néel temperature,²⁴ making it attractive for magnonics and spintronics.

In its bulk form, CrSBr possesses an orthorhombic structure (space group Pmmn; no. 59).²⁵ Below the Néel temperature (~ 132 K²⁴) the stacked layers couple antiferromagnetically and, within each layer, the spins are aligned along the b -axis (Fig. 1a), which is the easy-axis for this material. The Cr³⁺ ions (ideal magnetic moment $S=3/2$; measured $3.09 \mu_B$ ²⁵) are surrounded by four S and two Br atoms, leading to a distorted octahedral environment that lifts the degeneracy of the occupied t_{2g} and unoccupied e_g orbitals. ARPES and vertex-corrected quasiparticle self-consistent GW (QSG \widehat{W}) calculations reveal the band edges are dominated by Cr d -states with some degree of mixing from the S and Br p -states.^{26,27} The low energy optical spectrum is dominated by Cr d - d transitions with two well characterized bright excitons at ~ 1.37 eV (X_A)²⁸ and ~ 1.76 eV (X_B).²⁹ Both excitons are strongly anisotropic, being extended along the b -axis but confined along the a -axis, which is attributed to the quasi-1D nature of charge localization in this material.^{28,30,31}

By contrast, the fundamental band gap of bulk CrSBr is less well established, although ARPES studies place a lower bound of ~ 1.85 eV on this value while self-consistent GW calculations place this value closer to 1.95 eV³¹ or 2.05 eV.²⁶ Nevertheless, it is clear that at least the X_A exciton is tightly bound even in the bulk material, which is a departure from the norm for other layered semiconductors where such strong exciton binding typically only becomes apparent in the 2D limit.^{32–35} This unusual behavior is again attributed to the quasi-1D nature of the charge distribution that results in reduced dielectric screening, with additional localization resulting from the antiferromagnetic ordering between layers that suppresses interlayer coupling.¹⁶

While experimental research on CrSBr has proceeded at a rapid pace along several fronts, accurate first-principles modeling is limited and based primarily on many-body perturbation theory (MBPT), specifically, self-consistent GW calculations that do not suffer from starting-point dependencies.^{26,27,31,32,36} In particular, the QSGW method has yielded electronic bandstructures and optical absorption spectra for bulk CrSBr that are in excellent qualitative and quantitative agreement with several experimental studies.^{26,27,32,36} Other first-principles studies have variously employed semilocal density functionals,^{37,38} hybrid density functionals,^{28,39} DFT+U,^{40,41} or single-shot GW^{28,42,43} and, while these studies correctly capture the semiconducting nature of bulk CrSBr, the fundamental gaps are consistently underestimated relative to ARPES measurements. Moreover, the optical absorption spectra calculated via the Bethe-Salpeter equation (BSE) subsequent to single-shot GW,^{28,42,43} tend to capture only the X_A exciton energy correctly but not the features at higher energies. Other studies have adopted approaches based on dynamical mean-field theory⁴⁴ or cluster models^{45,46} that address the correlated nature of the Cr $3d$ orbitals and focus on understanding specific aspects of Cr $d-d$ transitions and Mott localization. It should be noted that these models are not entirely parameter free. Collectively, the first-principles

calculations that have been performed to date raise a fundamental question: can the electronic structure and optical response of bulk CrSBr be modeled with *quantitative* accuracy within the framework of generalized Kohn-Sham (GKS) time-dependent density functional theory (TDDFT) or are MBPT and/or quantum chemistry-based methods unavoidable? Indeed, if one is able to harness the conventional machinery of TDDFT for CrSBr (and, possibly, similar magnetic semiconductors), this would alleviate a fair amount of computational expense and, moreover, allow for routine calculations in widely-used first-principles codes.

The purpose of this paper is to demonstrate that it is possible to design a simple tuned hybrid density functional that can capture most of the known electronic and optical features of bulk CrSBr, as well as the coupling of these features to magnetic order, with *high accuracy*. Specifically, we show that by tuning a hybrid functional (whose form we specify later) to capture the X_A and X_B exciton energies of bulk CrSBr, we are able to obtain excellent qualitative agreement for the nature of the band edges as well as quantitative estimates for the fundamental gap that agree well with ARPES and QSGW results. Using this tuned functional, we also study coupling of excitons to the magnetic order and obtain quantitatively accurate estimates for the shifts in the X_A and X_B exciton energies, as well as changes in oscillator strengths and emergence of satellite peaks in the excitonic spectrum. More broadly, our work suggests that GKS-TDDFT can potentially be extended to model the optoelectronic response of other magnetic semiconductors, complementing and simplifying the state-of-the-art in the field.

2. RESULTS AND DISCUSSION

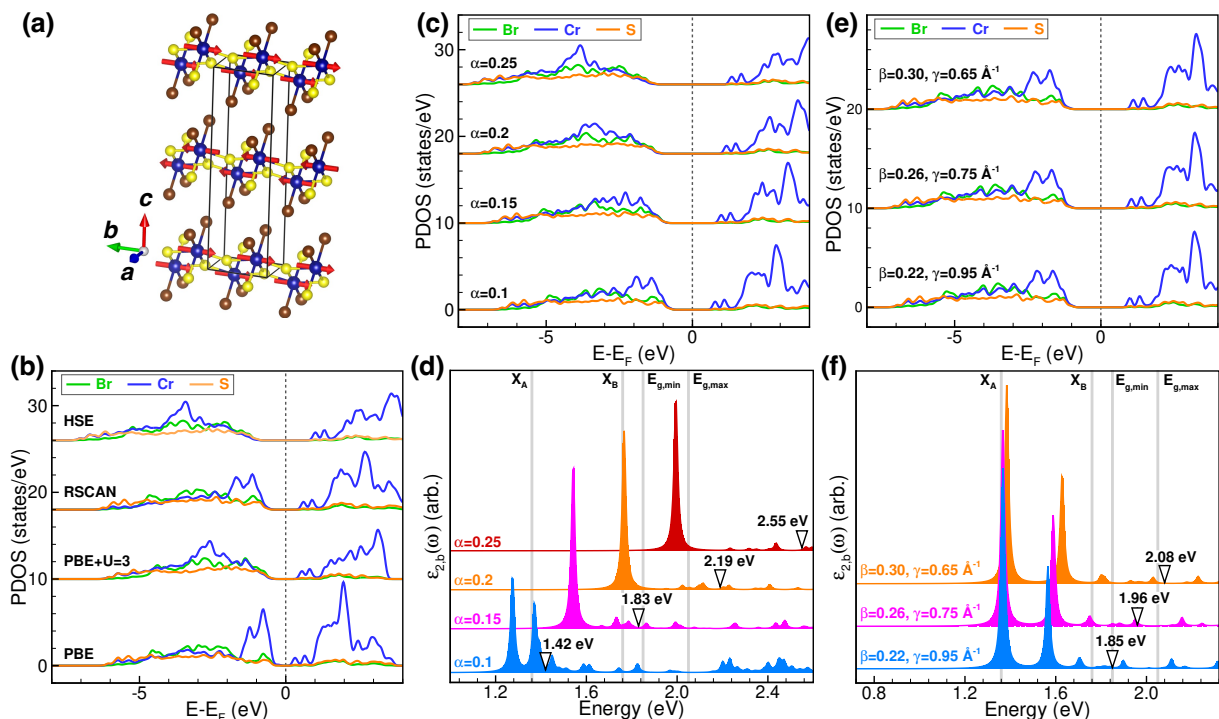


Figure 1: (a) Crystal structure of bulk CrSBr; Cr, S, Br are indicated by blue, yellow, and brown spheres, respectively, and the magnetic moments (AFM state) are indicated by red arrows. (b) Species-wise projected density of states (PDOS) using selected density functionals. (c) Species-wise PDOS using global hybrids with varying fractions of exact exchange and (d) their calculated optical spectra (imaginary part of the dielectric function) along the b -axis. (e, f) Same as (c, d) but with range-separated hybrids consisting of 100% semilocal exchange (PBE) in the short range and a fraction β of exact-exchange in the long range, γ being the range-separation parameter. In (d) and (f), we have marked by grey vertical lines the reference energies of the X_A (1.36 eV) and X_B (1.76 eV) excitons as well as the approximate bounds on the fundamental gap ($E_{g,\min}=1.85$ eV and $E_{g,\max}=2.05$ eV); the fundamental gaps are indicated by inverted triangles. The Fermi level is set mid-gap in all PDOS plots and only the majority spin PDOS are indicated, the minority spin states being degenerate.

To inform the design of a suitable hybrid functional, we begin by examining the *qualitative* behavior of a few different density functionals, our goal being to understand how the character of the band edges, fundamental gaps, and optical absorption spectra evolve with varying treatments of exchange. Figure 1(b) displays the species-wise projected density of states for two semilocal functionals – PBE⁴⁷ and the RSCAN metaGGA⁴⁸ – as well as PBE+ U and the HSE⁴⁹ functional (that only contains short-range exact exchange). Both PBE and RSCAN predict that the valence

band edge is dominated by Cr (d -states) with some mixing from S and Br states, and this agrees well with QSG \widehat{W} and DMFT calculations.^{26,44} In contrast, both PBE+ U (for which we use $U=3$ eV, as an example) and HSE shift the Cr states to lower energies, leading to much greater mixing of anion p - and cation d -states at the valence band edge. The similar behavior of PBE+ U and HSE can be understood by recognizing that the U correction effectively provides a simplified screened Fock-like exchange in the short-range,⁵⁰⁻⁵² the difference being that the U correction is applied only to a selected subspace (here, Cr d -orbitals) whereas in HSE the short-range exact exchange is applied to all orbitals. In all cases though, the conduction band edge is predominantly of Cr character with the clear presence of two peaks at the band edge that correspond to the well-known flat conduction bands along the $\Gamma - X$ direction (crystallographic a axis).²⁸ These results provide the first useful hint that the inclusion of short-range exact exchange can, perhaps unexpectedly, lead to a qualitatively incorrect description of the valence band edge. However, we cannot yet determine the impact on the excitonic properties, as these functionals lack the proper long range behavior required for obtaining bound excitons.^{53,54}

Thus, we consider next hybrid functionals that contain long-range exact exchange, beginning with global hybrids where the exchange potential, v_x , is given by

$$v_x = \alpha v_{XX} + (1 - \alpha)v_{SL}, \quad (1)$$

where α is the fraction of exact exchange (XX) and $1 - \alpha$ is the fraction of semilocal (SL) exchange. We use PBE semilocal exchange and correlation throughout this work. Figure 1(c) displays the PDOS for fractions of exact exchange ranging from 10–25% from which we once again observe that with increasing fraction of exact exchange the Cr states shift progressively deeper into the valence band, which is undesirable. The fundamental gap increases linearly with increasing exact exchange (Fig. S1). The optical absorption spectra are displayed in Figure 1(d)

from which we note two significant features: first, the absorption onset (defined as the energy of the first excitonic peak) is blue-shifted with increasing exact exchange and, second, the satellite peaks that are 0.2–0.3 eV above the first peak are correspondingly rapidly suppressed. The blue shift of the first exciton peak is again nearly linear correlated with the fraction of exact exchange (Fig. S1) although at a slower rate than the fundamental gap, leading to stronger exciton binding with increasing exact exchange. Looking specifically at the case of $\alpha = 0.15$, for which the fundamental gap (1.83 eV) is nearly at the lower bound (1.85 eV), it is already apparent that the first excitonic peak is substantially higher (~ 0.2 eV) than that of the X_A exciton and, moreover, the spectral features in the vicinity of the X_B exciton range are greatly suppressed.

Clearly, while global hybrids are unable to describe bulk CrSBr correctly, the earlier observation that semilocal functionals appear to capture the qualitative character of the valence band edge correctly suggest the possibility of employing a screened range-separated hybrid (SRSH) functional^{34,35,55–57} wherein short-range exact exchange is minimized while a fraction of long-range exact exchange is retained to ensure correct dielectric screening. As an extreme case, we consider one such form for an SRSH where the exchange potential, v_x , is given by

$$v_x = v_{SL}^{SR} + \beta v_{XX}^{LR} + (1 - \beta)v_{SL}^{LR}, \quad (2)$$

such that the short-range (SR) component is purely semilocal, switching to a long-range (LR) component that admixes a fraction, β , of exact exchange with a complementary fraction, $1 - \beta$, of semilocal (PBE) exchange. Treating β and the range-separation parameter, γ , as tunable parameters, we calculated the electronic structure and optical spectra with the aim of finding suitable $\beta - \gamma$ pairs for which the X_A exciton energy is close to the reference value while the fundamental gap is within the acceptable bounds. Figures 1(e, f) show the outcomes of these calculations for a few select cases from which it is clear that suppressing short-range exact

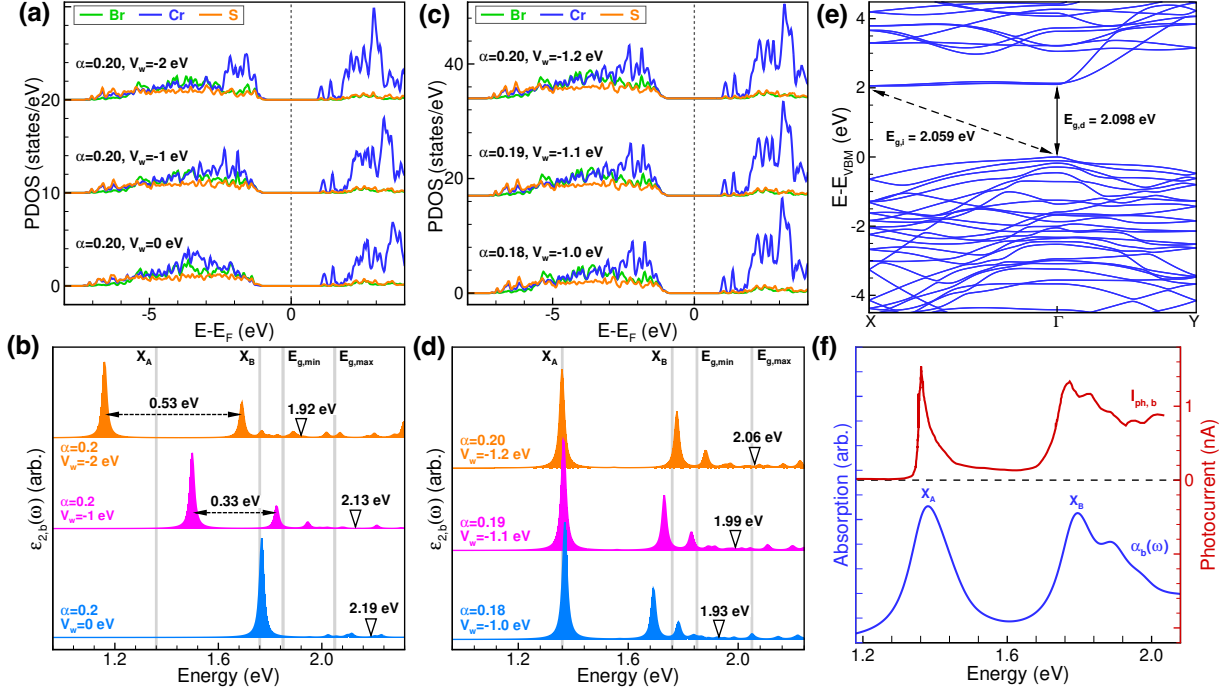


Figure 2: (a) Species-wise PDOS of bulk CrSBr using the hybrid+ V_w approach and (b) the corresponding optical spectra (imaginary part of the dielectric function) along the b -axis. (c, d) Same as (a, b) but with the inclusion of spin-orbit coupling, and (e) the Wannier-interpolated bandstructure for the case of $\alpha = 0.2$ and $V_w = -1.2$ eV. The fundamental gap is weakly indirect between the Γ and X points. (f) Comparison of the photocurrent spectrum ($I_{\text{ph},b}$) measured for incident light polarized along the b -axis, extracted from Ref. 62, and the calculated absorption spectrum [$\alpha_b(\omega) \propto \omega \kappa_b(\omega)$; $\kappa_b(\omega)$ is the extinction coefficient] using $\alpha = 0.2$ and $V_w = -1.2$ eV, and a broadening of 50 meV. In (b) and (d), we have marked by grey vertical lines the reference energies of the X_A (1.36 eV) and X_B (1.76 eV) excitons as well as the approximate bounds on the fundamental gap ($E_{g,\text{min}}=1.85$ eV and $E_{g,\text{max}}=2.05$ eV); the fundamental gaps are indicated by inverted triangles. The Fermi level is set mid-gap in all PDOS plots and only the majority spin PDOS are indicated in (a), the minority spin states being degenerate.

exchange indeed produced band edges that are predominantly composed of Cr states with low mixing of S and Br states. It is also clear that the energy of the X_B exciton is much lower than desired even though the oscillator strength is significantly higher than with pure global hybrids. These conclusions also hold good for more general cases where a small fraction of exact exchange was included in the short-range (see Fig. S2 for an example). Altogether, these failures do provide one systematic and key insight: while exact-exchange is generally beneficial for mitigating self-interaction errors, it is actually detrimental in the present situation for the Cr d -orbitals, causing *over-localization*. Put differently, we need to consider *orbital-wise* corrections and treat the s - and

p -states of the anions differently from the correlated Cr d -orbitals, and this consideration motivates the final approach we describe here based on combining (global) hybrid functionals with on-site corrections, the so-called “hybrid+ V_w ” method.^{58–60}

The hybrid+ V_w method was proposed by Ivády *et al.*^{58–60} as a way to introduce orbital-wise corrections within the framework of hybrid DFT, aimed at alleviating inaccuracies that arise in correlated systems from treating localized and extended states on the same footing vis-à-vis screening. Specifically, they showed that within the fully-localized limit, hybrid DFT can be viewed as analogous to DFT+ U where the strength of the on-site potential for the former is now directly proportional to the fraction of exact exchange, α . Viewed in this light, it is not surprising that the homogeneous screening provided by a single value of α might not be appropriate for localized versus extended states, much as different states require different U corrections in the DFT+ U method. Thus, Ivády *et al.* augmented the global hybrid potential (Eq. 1) with an additional on-site potential of the form⁵⁹

$$V_m^\sigma = w \left(\frac{1}{2} - n_m^\sigma \right), \quad (3)$$

that is applied selectively to a set of localized atomic-like orbitals φ_m^σ , w being the strength of the on-site potential and n_m^σ being the on-site occupation matrix. The form of this potential is motivated by the simplified rotationally-invariant form of DFT+ U proposed by Dudarev *et al.*⁶¹ Note that the parameter w can take on either positive or negative values and can be determined, in principle, by satisfying the ionization potential theorem, e.g., for defect states of transition-metal dopants in semiconductors.^{58,59} For the present, we treat α and w as adjustable parameters that are tuned to obtain the desired energies of the X_A and X_B excitons while fulfilling the bounds on the fundamental gap.

Figure 2(a) displays the outcome of the hybrid+ V_w method, applied to bulk CrSBr (AFM phase), where we fix the fraction of exact exchange ($\alpha = 0.20$) and vary the onsite potential, V_w . As evident, applying negative values of V_w to the Cr d -orbitals systematically cancels out the excess exact exchange acting on these orbitals, shifts these states progressively towards the valence band edge, reduces the extent of p - d mixing (qualitatively in line with QSGW and DMFT calculations), and reduces the fundamental band gap. Moreover, as seen from Figure 2(b), the X_A excitonic peak shift to lower energies while the X_B excitonic peak acquires more intensity as the Cr character of the valence edges increases. Most interestingly, it is now possible to control the splitting between the X_A and X_B excitons, unlike with SRSH functionals where the splitting remains in the range of 0.2–0.3 eV if the fundamental gap is to stay within acceptable bounds. Based on this insight, we systematically tuned α and V_w – now with full inclusion of spin-orbit coupling and Cr magnetic moments correctly aligned (antiferromagnetically) along the easy b -axis – and the outcome of these calculations is displayed for select cases in Figure 2(c) and (d). Specifically, in the tuning procedure, we demand first that the energy of the X_A excitonic peak is as close as possible to the correct reference energy and then further require that the X_B excitonic peak is also close to its reference value while ensuring that the fundamental gap stays within acceptable bounds. The choice of parameters is, of course, not unique but we choose $\alpha = 0.2$ and $V_w = -1.2$ eV as a representative case for now. Figure 2(e) displays the electronic bandstructure from which we note the nearly flat pair of bands along the $\Gamma - X$ direction^{16,28} at the conduction band edge and we also find the fundamental gap to be weakly indirect. Figure 2(f) displays a comparison between the photocurrent spectrum for light polarized along the b -axis, reported in Ref. 62, and our calculated absorption coefficient for the same direction, which we find to be in excellent agreement, both with respect to peak positions and intensities.

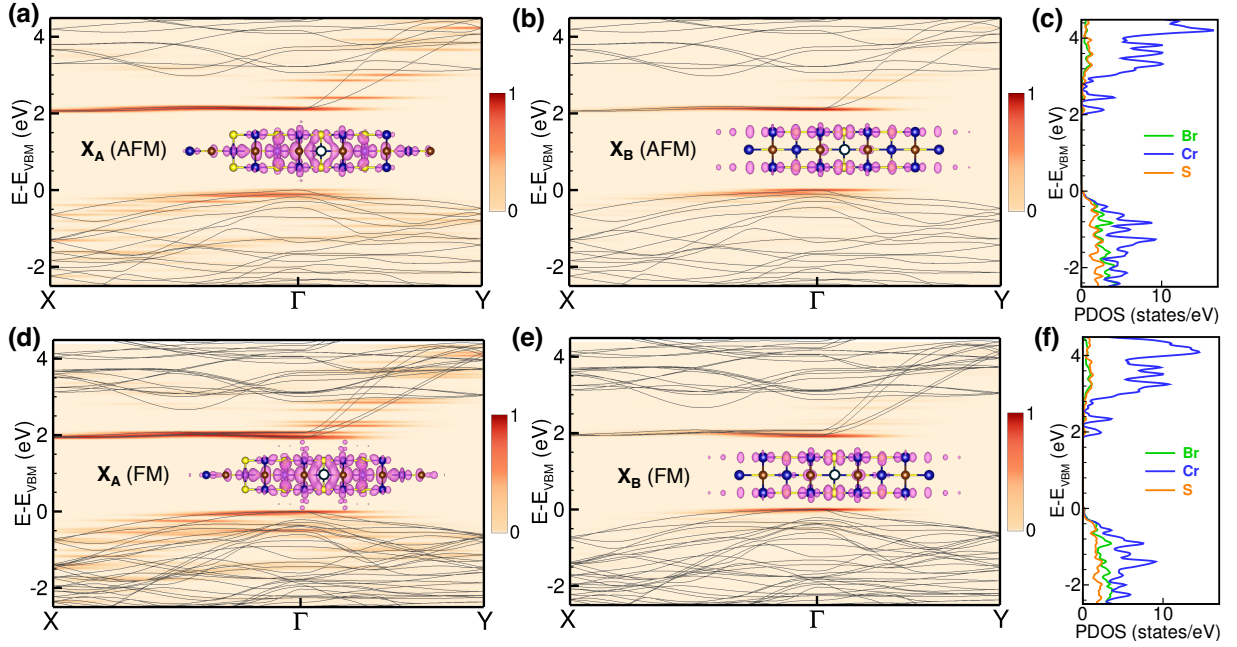


Figure 3: (a, b) Wannier-interpolated bandstructure of bulk CrSBr (AFM phase) with superposed heatmaps indicating the contributions from the bands to the X_A and X_B excitons. Insets depict the real-space charge density of the two excitons, with the hole position being fixed in the vicinity of a Cr atom (white circle). (c) Species-wise PDOS for the bulk AFM phase. (c, d, e) Same as (a, b, c) but for the bulk ferromagnetic (c-FM) phase with Cr magnetic moments aligned along the c -axis. All calculations are performed with $\alpha = 0.2$ and $V_w = -1.2$ eV, and with the inclusion of spin-orbit coupling.

To gain further insight into the composition and nature of the excitons, we display in Figures 3(a, b) the bandstructures of the bulk AFM phase and indicate via heatmaps (derived from BSE fatbands, as explained in Sec. S3) the contributions of the bands to the X_A and X_B excitons, respectively. Unlike the X_B exciton that is composed largely of band-edge states, the X_A exciton has more contributions from states deeper in the valence and conduction bands and is also more spread out in reciprocal space. The tighter-bound X_A exciton is more localized in real space than the X_B exciton and both are strongly anisotropic, being elongated along the b -axis and confined along the a -axis. Both excitons have large Cr $d-d$ contributions with some $p-d$ character, as seen from their charge density distributions. We are unable at present to disentangle further the onsite vs. intersite nature of the $d-d$ excitations.³⁶

Up to this point, we have demonstrated that the hybrid+ V_w functional can be tuned to reproduce a couple of known targets and, subsequently, produce bandstructures and absorption spectra that agree well with the literature. A more stringent test is to assess how well the functional predicts coupling of magnetic order to electronic structure, specifically, shifts in exciton energies under magnetic fields that are well characterized in experiments.^{29,36,42} Figure 4 displays the calculated optical spectra as a function of canting of Cr spins out of plane, effectively mimicking a gradually increasing external magnetic field (applied along the c -axis) that causes spins to eventually align ferromagnetically along the c -axis (see Computational Methods). Two features are particular noteworthy from these calculations: first, the X_A exciton redshifts by 38 meV whereas the X_B exciton redshifts more substantially by 132 meV; second, there is a progressive redistribution of spectral weight between the X_B exciton and its satellite peaks (originally in the ~ 1.8 – 2.0 eV range) leading ultimately to three peaks (X_B, X'_B, X''_B ³⁶) of similar intensities in the FM phase. The fundamental gap of the c -FM phase is calculated to be 1.92 eV, a decrease of 0.14 eV relative to

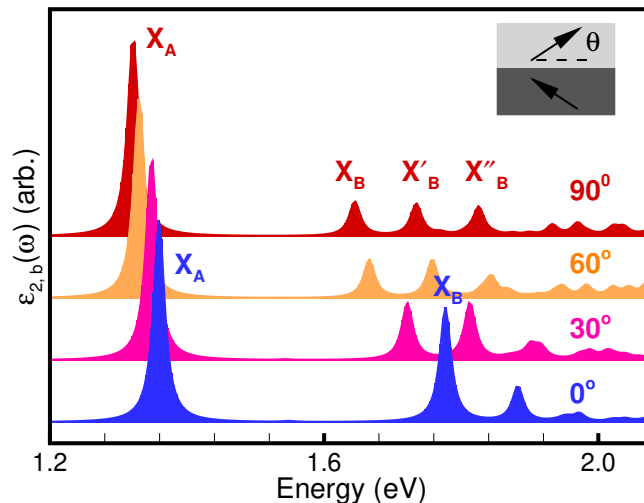


Figure 4: Optical spectra (imaginary part of the dielectric function) along the b -axis as a function of orientation of Cr spins. Starting from the blue spectrum (AFM case) the Cr spins progressively cant out of plane (in steps of 30°) until they are completely ferromagnetically aligned normal to the layers (along the c -axis).

the AFM phase, which is in excellent agreement QSGW results.³⁶ This reduction in band gap occurs as interlayer hopping is no longer spin-forbidden for the c-FM case, unlike the AFM case.^{16,29} The redshift of the X_B exciton then nearly tracks the change in fundamental gap, being composed mostly of band edge states (Fig. 3e), whereas the more-localized X_A exciton, which is composed of deeper states (Fig. 3d), is less affected by overall changes in the fundamental gap. This is consistent with Śmiertka *et al.*'s³⁶ finding that the X_A exciton has larger contributions from onsite d - d transitions, making them less sensitive to band-structure changes, although we are unable to verify this at present in our calculations. Overall, the calculated redshifts of the X_A and X_B excitons, while slightly higher than measured ones (X_A : 20 meV,⁶³ 14 ± 2 meV,²¹ ~ 12 meV³⁶; X_B : 110 meV,³⁶ ~ 100 meV²⁹), are nevertheless in reasonable agreement. We note that the unit cell is frozen in these simulations and magnetostriction should ideally be accounted for in the future to refine the calculated shifts.

3. CONCLUSIONS

To conclude, we have presented a simple yet effective approach for calculating the electronic and optical properties of bulk CrSBr with quantitative accuracy. By merging a global hybrid functional, which allows for mitigation of self-interaction errors and for proper long-range dielectric screening, with on-site potential corrections (V_w) applied selectively to mitigate over-localization of correlated Cr d -states, we have shown that it is possible to model this complex magnetic semiconductor within the framework of GKS TDDFT. Not only is the hybrid+ V_w approach advantageous by way of computational cost relative to state-of-the-art MBPT calculations but it is also fully variational and based on methods (hybrid DFT and DFT+U) that are widespread in first-principles codes. This allows for straightforward calculations, for example, of magneto-crystalline

anisotropy and exchange coupling constants that can be used to study spin dynamics in the future. Moreover, relying only on two parameters, the functional can be tuned in a straightforward manner to reproduce a minimal number of experimental and/or theoretical benchmarks (e.g., fundamental/optical gaps), thereafter, delivering excellent predictive capability. While the need for empirical tuning is certainly a drawback relative to fully *ab initio* approaches, the necessary parameters could potentially be determined in the future using optimal-tuning procedures that have been developed recently for the solid state.^{35,55,64–66} Lastly, it would be interesting to understand systematically how the hybrid+ V_w approach performs for weakly- vs. strongly-correlated systems, more precisely, to what extent (single-determinant) GKS theory can capture the essential physics as multi-determinant contributions become dominant and whether it can be combined effectively with DMFT in these situations.

COMPUTATIONAL METHODS

All calculations were performed using the Vienna *Ab Initio* Simulation Package (VASP).^{67,68} Standard projector-augmented-wave (PAW) potentials⁶⁹ provided with VASP were used to model core and valence electrons. The valence configurations of Cr, S, Br are $3p^64s^13d^5$, $3s^23p^4$, and $4s^24p^5$, respectively. Semilocal contributions to electron exchange and correlation were modeled using the Perdew-Burke-Ernzerhof (PBE)⁴⁷ form of the generalized-gradient approximation in correspondence with the PAW potentials. The kinetic energy cutoff was set to 550 eV, and the Brillouin zone was sampled using a $10 \times 8 \times 2$ Γ -centered k -point mesh. A Gaussian smearing of 50 meV was used in all calculations. Linear-response TDDFT calculations⁷⁰ were performed in the Tamm-Dancoff approximation,⁷¹ using 60 occupied and 20 unoccupied bands (as determined from convergence tests). Gaussian broadening of 10 meV was used for all optical spectra except

when comparing to experiments (Fig. 2f) where 50 meV broadening was used to facilitate better comparison. Calculations with canted spins were performed using the constrained magnetization implementation in VASP and only the orientations of the spins were fixed at desired canting angles. SRSB calculations were performed using our own custom implementation, while hybrid+ V_w calculations were performed by merging hybrid DFT and DFT+U (rotationally-invariant form of Dudarev *et al.*⁶¹) tags in the VASP input file. Atomic positions and lattice parameters were fixed at their experimental values²⁵ (see Sec. S2). Selected tests, verifying the hybrid+ V_w approach with the SIESTA package, are provided in Section S4.

ACKNOWLEDGEMENTS

A.R. thanks Dr. Swagata Acharya and Prof. Leeor Kronik for several insightful discussions. A.R. also gratefully acknowledges computational support from the Office of Information Technology at the University of Massachusetts Amherst and the Massachusetts Green High-Performance Computing Center. D.H.-P. is grateful for funding from the Diputación Foral de Gipuzkoa through Grants 2023-FELL-000002-01, 2024-FELL-000009-01, and 2025-FELL-000004-01 and Red Guipuzcoana R&D Project TRAFIC (Project 2025-CIE4-000036-01). D.H.-P. is also grateful for the support of the Spanish MICIU/AEI/10.13039/501100011033 and by ERDF/UE, through grant PID2023-147324NA-I00 and from IKUR Strategy, Quantum Technologies 2025 project M-Twist, from the Department of Science, Universities and Innovation of the Basque Government. J.J. acknowledges financial support from Grant No.~PID2022-139776NB-C63 funded by MCIN/AEI/10.13039/501100011033 and by ERDF “A way of making Europe” by the European Union. M.C.-G. acknowledges support from the Diputación Foral de Gipuzkoa through grants 2024-FELL-000007-01 and 2025-FELL-000009-01, and from grant no. PID2024-159869NA-

I00 funded by MICIU/AEI/10.13039/501100011033 and ERDF/EU. D.H.-P. and M.C.-G. thankfully acknowledge RES resources provided by the Barcelona Supercomputing Center in MareNostrum 5 to FI-2024-2-0023, FI-2024-3-0024.

SUPPORTING INFORMATION

Supporting figures for global and range-separated hybrids; unit cell and atomic coordinates of bulk CrSBr; exciton fatband plots; selected tests of the hybrid+ V_w approach with the SIESTA package

REFERENCES

- (1) Gibertini, M.; Koperski, M.; Morpurgo, A. F.; Novoselov, K. S. Magnetic 2D Materials and Heterostructures. *Nature Nanotechnology* **2019**, *14* (5), 408–419. <https://doi.org/10.1038/s41565-019-0438-6>.
- (2) Mannix, A. J.; Kiraly, B.; Hersam, M. C.; Guisinger, N. P. Synthesis and Chemistry of Elemental 2D Materials. *Nature Reviews Chemistry* **2017**, *1* (2), 0014. <https://doi.org/10.1038/s41570-016-0014>.
- (3) Huang, X.; Wang, T.; Miao, S.; Wang, C.; Li, Z.; Lian, Z.; Taniguchi, T.; Watanabe, K.; Okamoto, S.; Xiao, D.; Shi, S.-F.; Cui, Y.-T. Correlated Insulating States at Fractional Fillings of the WS₂/WSe₂ Moiré Lattice. *Nature Physics* **2021**, *17* (6), 715–719. <https://doi.org/10.1038/s41567-021-01171-w>.
- (4) Cao, Y.; Fatemi, V.; Fang, S.; Watanabe, K.; Taniguchi, T.; Kaxiras, E.; Jarillo-Herrero, P. Unconventional Superconductivity in Magic-Angle Graphene Superlattices. *Nature* **2018**, *556* (7699), 43–50. <https://doi.org/10.1038/nature26160>.
- (5) Xia, F.; Wang, H.; Xiao, D.; Dubey, M.; Ramasubramaniam, A. Two-Dimensional Material Nanophotonics. *Nature Photonics* **2014**, *8* (12), 899–907.
- (6) Zhou, X.; Hu, X.; Yu, J.; Liu, S.; Shu, Z.; Zhang, Q.; Li, H.; Ma, Y.; Xu, H.; Zhai, T. 2D Layered Material-Based van Der Waals Heterostructures for Optoelectronics. *Advanced Functional Materials* **2018**, *28* (14), 1706587. <https://doi.org/10.1002/adfm.201706587>.
- (7) Lin, Z.; McCreary, A.; Briggs, N.; Subramanian, S.; Zhang, K.; Sun, Y.; Li, X.; Borys, N. J.; Yuan, H.; Fullerton-Shirey, S. K.; Chernikov, A.; Zhao, H.; McDonnell, S.; Lindenberg, A. M.; Xiao, K.; LeRoy, B. J.; Drndić, M.; Hwang, J. C. M.; Park, J.; Chhowalla, M.; Schaak, R. E.; Javey, A.; Hersam, M. C.; Robinson, J.; Terrones, M. 2D Materials Advances: From Large Scale Synthesis and Controlled Heterostructures to Improved Characterization Techniques, Defects and Applications. *2D Materials* **2016**, *3* (4), 042001. <https://doi.org/10.1088/2053-1583/3/4/042001>.
- (8) Dirnberger, F.; Bushati, R.; Datta, B.; Kumar, A.; MacDonald, A. H.; Baldini, E.; Menon, V. M. Spin-Correlated Exciton–Polaritons in a van Der Waals Magnet. *Nature Nanotechnology* **2022**, *17* (10), 1060–1064. <https://doi.org/10.1038/s41565-022-01204-2>.

- (9) Lachance-Quirion, D.; Tabuchi, Y.; Gloppe, A.; Usami, K.; Nakamura, Y. Hybrid Quantum Systems Based on Magnonics. *Applied Physics Express* **2019**, *12* (7), 070101. <https://doi.org/10.7567/1882-0786/ab248d>.
- (10) Zhang, X.; Zou, C.-L.; Jiang, L.; Tang, H. X. Strongly Coupled Magnons and Cavity Microwave Photons. *Phys. Rev. Lett.* **2014**, *113* (15), 156401. <https://doi.org/10.1103/PhysRevLett.113.156401>.
- (11) Tabuchi, Y.; Ishino, S.; Noguchi, A.; Ishikawa, T.; Yamazaki, R.; Usami, K.; Nakamura, Y. Coherent Coupling between a Ferromagnetic Magnon and a Superconducting Qubit. *Science* **2015**, *349* (6246), 405–408. <https://doi.org/10.1126/science.aaa3693>.
- (12) Bae, Y. J.; Wang, J.; Scheie, A.; Xu, J.; Chica, D. G.; Diederich, G. M.; Cenker, J.; Ziebel, M. E.; Bai, Y.; Ren, H.; Dean, C. R.; Delor, M.; Xu, X.; Roy, X.; Kent, A. D.; Zhu, X. Exciton-Coupled Coherent Magnons in a 2D Semiconductor. *Nature* **2022**, *609* (7926), 282–286. <https://doi.org/10.1038/s41586-022-05024-1>.
- (13) Belvin, C. A.; Baldini, E.; Ozel, I. O.; Mao, D.; Po, H. C.; Allington, C. J.; Son, S.; Kim, B. H.; Kim, J.; Hwang, I.; Kim, J. H.; Park, J.-G.; Senthil, T.; Gedik, N. Exciton-Driven Antiferromagnetic Metal in a Correlated van Der Waals Insulator. *Nature Communications* **2021**, *12* (1), 4837. <https://doi.org/10.1038/s41467-021-25164-8>.
- (14) Yuan, H. Y.; Cao, Y.; Kamra, A.; Duine, R. A.; Yan, P. Quantum Magnonics: When Magnon Spintronics Meets Quantum Information Science. *Physics Reports* **2022**, *965*, 1–74. <https://doi.org/10.1016/j.physrep.2022.03.002>.
- (15) Diederich, G. M.; Cenker, J.; Ren, Y.; Fonseca, J.; Chica, D. G.; Bae, Y. J.; Zhu, X.; Roy, X.; Cao, T.; Xiao, D.; Xu, X. Tunable Interaction between Excitons and Hybridized Magnons in a Layered Semiconductor. *Nature Nanotechnology* **2023**, *18* (1), 23–28. <https://doi.org/10.1038/s41565-022-01259-1>.
- (16) Wilson, N. P.; Lee, K.; Cenker, J.; Xie, K.; Dismukes, A. H.; Telford, E. J.; Fonseca, J.; Sivakumar, S.; Dean, C.; Cao, T.; Roy, X.; Xu, X.; Zhu, X. Interlayer Electronic Coupling on Demand in a 2D Magnetic Semiconductor. *Nat. Mater.* **2021**, *20* (12), 1657–1662. <https://doi.org/10.1038/s41563-021-01070-8>.
- (17) Ziebel, M. E.; Feuer, M. L.; Cox, J.; Zhu, X.; Dean, C. R.; Roy, X. CrSBr: An Air-Stable, Two-Dimensional Magnetic Semiconductor. *Nano Lett.* **2024**. <https://doi.org/10.1021/acs.nanolett.4c00624>.

- (18) Marques-Moros, F.; Boix-Constant, C.; Mañas-Valero, S.; Canet-Ferrer, J.; Coronado, E. Interplay between Optical Emission and Magnetism in the van Der Waals Magnetic Semiconductor CrSBr in the Two-Dimensional Limit. *ACS Nano* **2023**, *17* (14), 13224–13231. <https://doi.org/10.1021/acsnano.3c00375>.
- (19) Tabataba-Vakili, F.; Nguyen, H. P. G.; Rupp, A.; Mosina, K.; Papavasileiou, A.; Watanabe, K.; Taniguchi, T.; Maletinsky, P.; Glazov, M. M.; Sofer, Z.; Baimuratov, A. S.; Högele, A. Doping-Control of Excitons and Magnetism in Few-Layer CrSBr. *Nature Communications* **2024**, *15* (1), 4735. <https://doi.org/10.1038/s41467-024-49048-9>.
- (20) Wang, T.; Zhang, D.; Yang, S.; Lin, Z.; Chen, Q.; Yang, J.; Gong, Q.; Chen, Z.; Ye, Y.; Liu, W. Magnetically-Dressed CrSBr Exciton-Polaritons in Ultrastrong Coupling Regime. *Nat Commun* **2023**, *14* (1), 5966. <https://doi.org/10.1038/s41467-023-41688-7>.
- (21) Li, Q.; Xie, X.; Alfrey, A.; Beach, C. W.; McLellan, N.; Lu, Y.; Hu, J.; Liu, W.; Dhale, N.; Lv, B.; Zhao, L.; Sun, K.; Deng, H. Two-Dimensional Magnetic Exciton Polariton with Strongly Coupled Atomic and Photonic Anisotropies. *Phys. Rev. Lett.* **2024**, *133* (26), 266901. <https://doi.org/10.1103/PhysRevLett.133.266901>.
- (22) Dirnberger, F.; Quan, J.; Bushati, R.; Diederich, G. M.; Florian, M.; Klein, J.; Mosina, K.; Sofer, Z.; Xu, X.; Kamra, A.; García-Vidal, F. J.; Alù, A.; Menon, V. M. Magneto-Optics in a van Der Waals Magnet Tuned by Self-Hybridized Polaritons. *Nature* **2023**, *620* (7974), 533–537. <https://doi.org/10.1038/s41586-023-06275-2>.
- (23) Long, F.; Ghorbani-Asl, M.; Mosina, K.; Li, Y.; Lin, K.; Ganss, F.; Hübner, R.; Sofer, Z.; Dirnberger, F.; Kamra, A.; Krasheninnikov, A. V.; Prucnal, S.; Helm, M.; Zhou, S. Ferromagnetic Interlayer Coupling in CrSBr Crystals Irradiated by Ions. *Nano Lett.* **2023**, *23* (18), 8468–8473. <https://doi.org/10.1021/acs.nanolett.3c01920>.
- (24) Göser, O.; Paul, W.; Kahle, H. G. Magnetic Properties of CrSBr. *Journal of Magnetism and Magnetic Materials* **1990**, *92* (1), 129–136. [https://doi.org/10.1016/0304-8853\(90\)90689-N](https://doi.org/10.1016/0304-8853(90)90689-N).
- (25) López-Paz, S. A.; Guguchia, Z.; Pomjakushin, V. Y.; Witteveen, C.; Cervellino, A.; Luetkens, H.; Casati, N.; Morpurgo, A. F.; von Rohr, F. O. Dynamic Magnetic Crossover at the Origin of the Hidden-Order in van Der Waals Antiferromagnet CrSBr. *Nat Commun* **2022**, *13* (1), 4745. <https://doi.org/10.1038/s41467-022-32290-4>.
- (26) Bianchi, M.; Acharya, S.; Dirnberger, F.; Klein, J.; Pashov, D.; Mosina, K.; Sofer, Z.; Rudenko, A. N.; Katsnelson, M. I.; van Schilfhaarde, M.; Rösner, M.; Hofmann, P.

- Paramagnetic Electronic Structure of CrSBr: Comparison between Ab Initio GW Theory and Angle-Resolved Photoemission Spectroscopy. *Phys. Rev. B* **2023**, *107* (23), 235107. <https://doi.org/10.1103/PhysRevB.107.235107>.
- (27) Watson, M. D.; Acharya, S.; Nunn, J. E.; Nagireddy, L.; Pashov, D.; Rösner, M.; van Schilfgaarde, M.; Wilson, N. R.; Cacho, C. Giant Exchange Splitting in the Electronic Structure of A-Type 2D Antiferromagnet CrSBr. *npj 2D Mater Appl* **2024**, *8* (1), 1–8. <https://doi.org/10.1038/s41699-024-00492-7>.
- (28) Klein, J.; Pingault, B.; Florian, M.; Heißenbüttel, M.-C.; Steinhoff, A.; Song, Z.; Torres, K.; Dirnberger, F.; Curtis, J. B.; Weile, M.; Penn, A.; Deilmann, T.; Dana, R.; Bushati, R.; Quan, J.; Luxa, J.; Sofer, Z.; Alù, A.; Menon, V. M.; Wurstbauer, U.; Rohlfing, M.; Narang, P.; Lončar, M.; Ross, F. M. The Bulk van Der Waals Layered Magnet CrSBr Is a Quasi-1D Material. *ACS Nano* **2023**, *17* (6), 5316–5328. <https://doi.org/10.1021/acsnano.2c07316>.
- (29) Nessi, L.; Occhialini, C. A.; Demir, A. K.; Powalla, L.; Comin, R. Magnetic Field Tunable Polaritons in the Ultrastrong Coupling Regime in CrSBr. *ACS Nano* **2024**, *18* (50), 34235–34243. <https://doi.org/10.1021/acsnano.4c11799>.
- (30) Klein, J.; Ross, F. M. Materials beyond Monolayers: The Magnetic Quasi-1D Semiconductor CrSBr. *Journal of Materials Research* **2024**, *39* (22), 3045–3056. <https://doi.org/10.1557/s43578-024-01459-6>.
- (31) Smolenski, S.; Wen, M.; Li, Q.; Downey, E.; Alfrey, A.; Liu, W.; Kondusamy, A. L. N.; Bostwick, A.; Jozwiak, C.; Rotenberg, E.; Zhao, L.; Deng, H.; Lv, B.; Zgid, D.; Gull, E.; Jo, N. H. Large Exciton Binding Energy in a Bulk van Der Waals Magnet from Quasi-1D Electronic Localization. *Nat Commun* **2025**, *16* (1), 1134. <https://doi.org/10.1038/s41467-025-56457-x>.
- (32) Shao, Y.; Dirnberger, F.; Qiu, S.; Acharya, S.; Terres, S.; Telford, E. J.; Pashov, D.; Kim, B. S. Y.; Ruta, F. L.; Chica, D. G.; Dismukes, A. H.; Ziebel, M. E.; Wang, Y.; Choe, J.; Bae, Y. J.; Millis, A. J.; Katsnelson, M. I.; Mosina, K.; Sofer, Z.; Huber, R.; Zhu, X.; Roy, X.; van Schilfgaarde, M.; Chernikov, A.; Basov, D. N. Magnetically Confined Surface and Bulk Excitons in a Layered Antiferromagnet. *Nat. Mater.* **2025**, *24* (3), 391–398. <https://doi.org/10.1038/s41563-025-02129-6>.

- (33) Ramasubramaniam, A. Large Excitonic Effects in Monolayers of Molybdenum and Tungsten Dichalcogenides. *Phys. Rev. B* **2012**, *86* (11), 115409. <https://doi.org/10.1103/PhysRevB.86.115409>.
- (34) Camarasa-Gómez, M.; Ramasubramaniam, A.; Neaton, J. B.; Kronik, L. Transferable Screened Range-Separated Hybrid Functionals for Electronic and Optical Properties of van Der Waals Materials. *Phys. Rev. Mater.* **2023**, *7* (10), 104001. <https://doi.org/10.1103/PhysRevMaterials.7.104001>.
- (35) Camarasa-Gómez, M.; Gant, S. E.; Ohad, G.; Neaton, J. B.; Ramasubramaniam, A.; Kronik, L. Excitations in Layered Materials from a Non-Empirical Wannier-Localized Optimally-Tuned Screened Range-Separated Hybrid Functional. *npj Comput Mater* **2024**, *10* (1), 1–9. <https://doi.org/10.1038/s41524-024-01478-1>.
- (36) Śmiertka, M.; Rygała, M.; Posmyk, K.; Peksa, P.; Dyksik, M.; Pashov, D.; Mosina, K.; Sofer, Z.; van Schilfgaarde, M.; Dirnberger, F.; Baranowski, M.; Acharya, S.; Plochocka, P. Distinct Magneto-Optical Response of Frenkel and Wannier Excitons in CrSBr. *Nature Communications* **2026**, *17* (1), 1777. <https://doi.org/10.1038/s41467-026-68482-5>.
- (37) Klein, J.; Pham, T.; Thomsen, J. D.; Curtis, J. B.; Denneulin, T.; Lorke, M.; Florian, M.; Steinhoff, A.; Wiscons, R. A.; Luxa, J.; Sofer, Z.; Jahnke, F.; Narang, P.; Ross, F. M. Control of Structure and Spin Texture in the van Der Waals Layered Magnet CrSBr. *Nat Commun* **2022**, *13* (1), 5420. <https://doi.org/10.1038/s41467-022-32737-8>.
- (38) Wang, Y.; Luo, N.; Zeng, J.; Tang, L.-M.; Chen, K.-Q. Magnetic Anisotropy and Electric Field Induced Magnetic Phase Transition in the van Der Waals Antiferromagnet CrSBr. *Phys. Rev. B* **2023**, *108* (5), 054401. <https://doi.org/10.1103/PhysRevB.108.054401>.
- (39) Liu, J.; Zhang, X.; Lu, G. Moiré Magnetism and Moiré Excitons in Twisted CrSBr Bilayers. *Proceedings of the National Academy of Sciences* **2025**, *122* (1), e2413326121. <https://doi.org/10.1073/pnas.2413326121>.
- (40) Feuer, M. L.; Thinel, M.; Huang, X.; Cui, Z.-H.; Shao, Y.; Chica, D. G.; Han, M.-G.; Pokratath, R.; Telford, E. J.; York, E.; Okuno, S.; Huang, C.-Y.; Bukula, O.; Nashabeh, L. M.; Qiu, S.; Nuckolls, C. P.; Dean, C. R.; Billinge, S. J. L.; Zhu, X.; Basov, D. N.; Millis, A. J.; Reichman, D. R.; Pasupathy, A. N.; Ziebel, M. E. Doping-Induced Charge Density Wave and Ferromagnetism in the Van Der Waals Semiconductor CrSBr.

- (41) Esteras, D. L.; Rybakov, A.; Ruiz, A. M.; Baldoví, J. J. Magnon Straintronics in the 2D van Der Waals Ferromagnet CrSBr from First-Principles. *Nano Lett.* **2022**, *22* (21), 8771–8778. <https://doi.org/10.1021/acs.nanolett.2c02863>.
- (42) Heißenbüttel, M.-C.; Piel, P.-M.; Klein, J.; Deilmann, T.; Wurstbauer, U.; Rohlfing, M. Quadratic Optical Response to a Magnetic Field in the Layered Magnet CrSBr. *Phys. Rev. B* **2025**, *111* (7), 075107. <https://doi.org/10.1103/PhysRevB.111.075107>.
- (43) Kalitukha, I. V.; Akimov, I. A.; Nestoklon, M. O.; Geirsson, T.; Molina-Sánchez, A.; Yalcin, E.; Ruppert, C.; Mayoh, D. A.; Balakrishnan, G.; Karuppasamy, M.; Sofer, Z.; Wang, Y.; Gillard, D. J.; Hu, X.; Tartakovskii, A. I.; Bayer, M. Magnetic Switching of Exciton Lifetime in CrSBr. arXiv January 8, 2026. <https://doi.org/10.48550/arXiv.2601.05413>.
- (44) Wu, F.; Zhang, X.; Chen, Y.; Pei, D.; Zhan, M.; Tao, Z.; Chen, C.; Lu, S.; Chen, J.; Tang, S.; Wang, X.; Guo, Y.; Yang, L.; Zhang, Y.; Chen, Y.; Mi, Q.; Li, G.; Liu, Z. Mott Insulating Phase and Coherent-Incoherent Crossover across Magnetic Phase Transition in 2D Antiferromagnetic CrSBr. *Sci. China Phys. Mech. Astron.* **2025**, *68* (6), 267411. <https://doi.org/10.1007/s11433-025-2625-7>.
- (45) Porée, V.; Zobelli, A.; Pawbake, A.; Regner, J.; Sofer, Z.; Faugeras, C.; Nicolaou, A. Resonant X-Ray Spectroscopies on CrSBr: Probing the Electronic Structure through Chromium d–d Excitations. *Phys. Rev. B* **2025**, *112* (12), 125103. <https://doi.org/10.1103/pdvz-6cpg>.
- (46) Sears, J.; Zager, B.; He, W.; Occhialini, C. A.; Shen, Y.; Lajer, M.; Villanova, J. W.; Berlijn, T.; Yakhou-Harris, F.; Brookes, N. B.; Chica, D. G.; Roy, X.; Baldini, E.; Pellicciari, J.; Bisogni, V.; Johnston, S.; Mitrano, M.; Dean, M. P. M. Observation of Anisotropic Dispersive Dark-Exciton Dynamics in CrSBr. *Phys. Rev. Lett.* **2025**, *135* (14), 146503. <https://doi.org/10.1103/fz3h-6jdx>.
- (47) Perdew, J. P.; Burke, K.; Ernzerhof, M. Generalized Gradient Approximation Made Simple. *Phys. Rev. Lett.* **1996**, *77* (18), 3865–3868. <https://doi.org/10.1103/PhysRevLett.77.3865>.
- (48) Bartók, A. P.; Yates, J. R. Regularized SCAN Functional. *The Journal of Chemical Physics* **2019**, *150* (16), 161101. <https://doi.org/10.1063/1.5094646>.

- (49) Krukau, A. V.; Vydrov, O. A.; Izmaylov, A. F.; Scuseria, G. E. Influence of the Exchange Screening Parameter on the Performance of Screened Hybrid Functionals. *The Journal of Chemical Physics* **2006**, *125* (22), 224106. <https://doi.org/10.1063/1.2404663>.
- (50) Anisimov, V. I.; Aryasetiawan, F.; Lichtenstein, A. I. First-Principles Calculations of the Electronic Structure and Spectra of Strongly Correlated Systems: The **LDA + U** Method. *J. Phys.: Condens. Matter* **1997**, *9* (4), 767–808. <https://doi.org/10.1088/0953-8984/9/4/002>.
- (51) Himmetoglu, B.; Floris, A.; de Gironcoli, S.; Cococcioni, M. Hubbard-Corrected DFT Energy Functionals: The LDA+U Description of Correlated Systems. *International Journal of Quantum Chemistry* **2014**, *114* (1), 14–49. <https://doi.org/10.1002/qua.24521>.
- (52) Macke, E.; Timrov, I.; Marzari, N.; Ciacchi, L. C. Orbital-Resolved DFT+U for Molecules and Solids. *J. Chem. Theory Comput.* **2024**, *20* (11), 4824–4843. <https://doi.org/10.1021/acs.jctc.3c01403>.
- (53) Yang, Z.; Ullrich, C. A. Direct Calculation of Exciton Binding Energies with Time-Dependent Density-Functional Theory. *Phys. Rev. B* **2013**, *87* (19), 195204. <https://doi.org/10.1103/PhysRevB.87.195204>.
- (54) Yang, Z.; Sottile, F.; Ullrich, C. A. Simple Screened Exact-Exchange Approach for Excitonic Properties in Solids. *Phys. Rev. B* **2015**, *92* (3), 035202. <https://doi.org/10.1103/PhysRevB.92.035202>.
- (55) Wing, D.; Ohad, G.; Haber, J. B.; Filip, M. R.; Gant, S. E.; Neaton, J. B.; Kronik, L. Band Gaps of Crystalline Solids from Wannier-Localization–Based Optimal Tuning of a Screened Range-Separated Hybrid Functional. *Proceedings of the National Academy of Sciences* **2021**, *118* (34), e2104556118. <https://doi.org/10.1073/pnas.2104556118>.
- (56) Wing, D.; Haber, J. B.; Noff, R.; Barker, B.; Egger, D. A.; Ramasubramaniam, A.; Louie, S. G.; Neaton, J. B.; Kronik, L. Comparing Time-Dependent Density Functional Theory with Many-Body Perturbation Theory for Semiconductors: Screened Range-Separated Hybrids and the GW plus Bethe-Salpeter Approach. **2019**, 1–15. <https://doi.org/10.1103/PhysRevMaterials.3.064603>.
- (57) Ramasubramaniam, A.; Wing, D.; Kronik, L. Transferable Screened Range-Separated Hybrids for Layered Materials: The Cases of MoS₂ and h-BN. *Physical Review Materials* **2019**, *3* (8), 084007.

- (58) Ivády, V.; Abrikosov, I. A.; Janzén, E.; Gali, A. Role of Screening in the Density Functional Applied to Transition-Metal Defects in Semiconductors. *Phys. Rev. B* **2013**, *87* (20), 205201. <https://doi.org/10.1103/PhysRevB.87.205201>.
- (59) Ivády, V.; Armiento, R.; Szász, K.; Janzén, E.; Gali, A.; Abrikosov, I. A. Theoretical Unification of Hybrid-DFT and DFT + U Methods for the Treatment of Localized Orbitals. *Phys. Rev. B* **2014**, *90* (3), 035146. <https://doi.org/10.1103/PhysRevB.90.035146>.
- (60) Ivády, V.; Gali, A.; Abrikosov, I. A. Hybrid-DFT + V_w Method for Band Structure Calculation of Semiconducting Transition Metal Compounds: The Case of Cerium Dioxide. *J. Phys.: Condens. Matter* **2017**, *29* (45), 454002. <https://doi.org/10.1088/1361-648X/aa8b93>.
- (61) Dudarev, S. L.; Botton, G. A.; Savrasov, S. Y.; Humphreys, C. J.; Sutton, A. P. Electron-Energy-Loss Spectra and the Structural Stability of Nickel Oxide: An LSDA+U Study. *Phys. Rev. B* **1998**, *57* (3), 1505. <https://doi.org/10.1103/PhysRevB.57.1505>.
- (62) Wu, F.; Gutiérrez-Lezama, I.; López-Paz, S. A.; Gibertini, M.; Watanabe, K.; Taniguchi, T.; von Rohr, F. O.; Ubrig, N.; Morpurgo, A. F. Quasi-1D Electronic Transport in a 2D Magnetic Semiconductor. *Advanced Materials* **2022**, *34* (16), 2109759. <https://doi.org/10.1002/adma.202109759>.
- (63) Heißenbüttel, M.-C.; Piel, P.-M.; Klein, J.; Deilmann, T.; Wurstbauer, U.; Rohlfing, M. Quadratic Optical Response of CrSBr Controlled by Spin-Selective Interlayer Coupling. arXiv March 29, 2024. <https://doi.org/10.48550/arXiv.2403.20174>.
- (64) Nguyen, N. L.; Colonna, N.; Ferretti, A.; Marzari, N. Koopmans-Compliant Spectral Functionals for Extended Systems. *Phys. Rev. X* **2018**, *8* (2), 021051. <https://doi.org/10.1103/PhysRevX.8.021051>.
- (65) Ma, J.; Wang, L.-W. Using Wannier Functions to Improve Solid Band Gap Predictions in Density Functional Theory. *Scientific Reports* **2016**, *6* (1), 24924. <https://doi.org/10.1038/srep24924>.
- (66) Ohad, G.; Camarasa-Gómez, M.; Neaton, J. B.; Ramasubramaniam, A.; Gould, T.; Kronik, L. Foundations of the Ionization Potential Condition for Localized Electron Removal in Density Functional Theory. *Phys. Rev. Lett.* **2026**, *136* (2), 026401. <https://doi.org/10.1103/ngyq-q7z3>.

- (67) Kresse, G.; Furthmüller, J. Efficient Iterative Schemes for Ab Initio Total-Energy Calculations Using a Plane-Wave Basis Set. *Phys. Rev. B* **1996**, *54* (16), 11169–11186. <https://doi.org/10.1103/PhysRevB.54.11169>.
- (68) Kresse, G.; Furthmüller, J. Efficiency of Ab-Initio Total Energy Calculations for Metals and Semiconductors Using a Plane-Wave Basis Set. *Computational Materials Science* **1996**, *6* (1), 15–50. [https://doi.org/10.1016/0927-0256\(96\)00008-0](https://doi.org/10.1016/0927-0256(96)00008-0).
- (69) Kresse, G.; Joubert, D. From Ultrasoft Pseudopotentials to the Projector Augmented-Wave Method. *Phys. Rev. B* **1999**, *59* (3), 1758–1775. <https://doi.org/10.1103/PhysRevB.59.1758>.
- (70) Casida, M. E. Time-Dependent Density Functional Response Theory for Molecules. In *Recent Advances in Density Functional Methods; Recent Advances in Computational Chemistry*; WORLD SCIENTIFIC, 1995; Vol. Volume 1, pp 155–192. https://doi.org/10.1142/9789812830586_0005.
- (71) Onida, G.; Reining, L.; Rubio, A. Electronic Excitations: Density-Functional versus Many-Body Green's-Function Approaches. *Rev. Mod. Phys.* **2002**, *74* (2), 601–659. <https://doi.org/10.1103/RevModPhys.74.601>.